

Targeting the CBM complex causes T_{reg} cells to prime tumours for immune checkpoint therapy

Mauro Di Pilato^{1,2,6*}, Edward Y. Kim^{1,2,6}, Bruno L. Cadilha¹, Jasper N. Prüssmann^{1,2}, Mazen N. Nasrallah^{1,2}, Davide Seruggia^{2,3}, Shariq M. Usmani^{1,2}, Sandra Misale^{2,4}, Valentina Zappulli⁵, Esteban Carrizosa^{1,2}, Vinidhra Mani^{1,2}, Matteo Ligorio^{2,4}, Ross D. Warner¹, Benjamin D. Medoff^{1,2}, Francesco Marangoni^{1,2}, Alexandra-Chloe Villani^{1,2} & Thorsten R. Mempel^{1,2*}

Solid tumours are infiltrated by effector T cells with the potential to control or reject them, as well as by regulatory T (T_{reg}) cells that restrict the function of effector T cells and thereby promote tumour growth¹. The anti-tumour activity of effector T cells can be therapeutically unleashed, and is now being exploited for the treatment of some forms of human cancer. However, weak tumour-associated inflammatory responses and the immune-suppressive function of T_{reg} cells remain major hurdles to broader effectiveness of tumour immunotherapy². Here we show that, after disruption of the CARMA1–BCL10–MALT1 (CBM) signalosome complex, most tumour-infiltrating T_{reg} cells produce IFN γ , resulting in stunted tumour growth. Notably, genetic deletion of both or even just one allele of *CARMA1* (also known as *Card11*) in only a fraction of T_{reg} cells—which avoided systemic autoimmunity—was sufficient to produce this anti-tumour effect, showing that it is not the mere loss of suppressive function but the gain of effector activity by T_{reg} cells that initiates tumour control. The production of IFN γ by T_{reg} cells was accompanied by activation of macrophages and upregulation of class I molecules of the major histocompatibility complex on tumour cells. However, tumour cells also upregulated the expression of PD-L1, which indicates activation of adaptive immune resistance³. Consequently, blockade of PD-1 together with CARMA1 deletion caused rejection of tumours that otherwise do not respond to anti-PD-1 monotherapy. This effect was reproduced by pharmacological inhibition of the CBM protein MALT1. Our results demonstrate that partial disruption of the CBM complex and induction of IFN γ secretion in the preferentially self-reactive T_{reg} cell pool does not cause systemic autoimmunity but is sufficient to prime the tumour environment for successful immune checkpoint therapy.

Local exposure of tumour-infiltrating T_{reg} cells to their cognate antigens sustains their tumour-promoting immunosuppressive functions⁴. We therefore explored which T-cell-receptor (TCR)-dependent signalling pathways could be targeted to disable tumour-reactive T_{reg} cells. The scaffold protein CARMA1 nucleates assembly of the CBM complex in T cells in response to TCR-dependent PKC θ activity and promotes several functions, including activation of the AP-1, mTOR and classical NF- κ B pathways, as well as stabilization of mRNA⁵. Constitutive genetic deletion of CARMA1, BCL10 or MALT1 abrogates thymic development of T_{reg} cells^{6–10}, but their role in mature T_{reg} cells is unknown.

When we conditionally deleted either one or both alleles of *CARMA1* in mature T_{reg} cells by crossing *Foxp3*^{YFP-cre} to *CARMA1*^{flox/flox} mice (hereafter referred to as *F^{cre} × C1^{f/+}* or *F^{cre} × C1^{ff/ff}* mice), levels of CARMA1 protein were proportionally reduced in CD4⁺FOXP3⁺ T_{reg} cells from lymph nodes (LNs) (Extended Data Fig. 1a). *F^{cre} × C1^{ff/ff}*, but not *F^{cre} × C1^{f/+}* or *C1^{f/+}* control mice, stopped thriving at 17 days; most died before 4 weeks of age after a T-helper-1 (T_H1)-dominated multiorgan inflammatory disease characterized by splenomegaly,

lymphadenopathy, effector differentiation and inflammatory cytokine secretion by conventional T (T_{conv}) cells, production of auto-reactive IgG, and activation of the myeloid compartment (Fig. 1a, Extended Data Figs. 1b–f, 2a–f). Hence, CARMA1 is essential for T_{reg} cells to maintain immune homeostasis, but a reduction in its expression at least up to 50% is tolerated.

Absolute numbers of T_{reg} cells were increased in LNs of *F^{cre} × C1^{ff/ff}* mice, concomitant with an increase in overall LN cellularity (Extended Data Fig. 2g, h). However, the overall frequency of T_{reg} cells among CD4⁺ T cells did not vary with CARMA1 expression, whereas the proportion of CD44^{high}CD62L[–] effector T_{reg} (eT_{reg}) was strongly reduced in its absence (Fig. 1b). Notably, CARMA1-deficient T_{reg} cells, while retaining expression of FOXP3, almost uniformly secreted IFN γ and—at lower frequencies—secreted IL-4, IL-17 and TNF (Fig. 1c). Although nearly all CARMA1-deficient T_{reg} cells secreted the T_H1-cytokine IFN γ , far fewer—and only eT_{reg} cells—expressed the T_H1 lineage-defining transcription factor T-bet along with ROR γ t and, to a lesser degree, GATA-3 (Fig. 1d and Extended Data Fig. 2i, j). Hence, complete—but not partial—deletion of CARMA1 in T_{reg} cells markedly dysregulates their cytokine expression that (in the case of IFN γ) is dissociated from expression of T-bet, and may contribute to the pathogenesis of inflammatory disease. Indeed, *F^{cre} × C1^{ff/ff}* mice died more rapidly than T_{reg} cell-deficient *scurfy* mice, but their lifespans were similar when IFN γ was neutralized (Fig. 1e). Thus, under inflammatory conditions, CARMA1-deficient T_{reg} cells convert from an immunoregulatory cell type into an IFN γ -secreting pathogenic cell type.

In heterozygous female *F^{cre} × C1^{ff/ff}* mice, random inactivation of the X chromosome causes the yellow fluorescent protein–Cre recombinase (YFP–Cre) fusion protein to be expressed and CARMA1 to be deleted in only half of the T_{reg} cells, whereas the other half maintains immune homeostasis (Extended Data Fig. 3a–c). Under such non-inflammatory conditions, CARMA1-deficient T_{reg} cells did not secrete effector cytokines (Fig. 1f). However, in competition with CARMA1-sufficient T_{reg} cells for niche space, we observed a proportional decline specifically in the frequency of eT_{reg} cells—but not of central T_{reg} (cT_{reg}) cells—that lacked one or both alleles of *CARMA1* (Fig. 1g and Extended Data Fig. 3e). The remaining YFP⁺ eT_{reg} cells expressed less FOXP3 and other proteins that are characteristically increased in expression during the differentiation of cT_{reg} cells into eT_{reg} cells (Fig. 1h). They expressed more of the pro-apoptotic protein BIM, but also more of the anti-apoptotic protein BCL2, which probably reflects impaired differentiation of eT_{reg} cells, as control eT_{reg} cells strongly downregulated both BCL2 and BIM relative to cT_{reg} cells (Extended Data Fig. 3d–h). The in vitro suppressive function of CARMA1-deficient T_{reg} cells was reduced, but not abrogated (Extended Data Fig. 4a, b), and they failed to persist and did not suppress lymphopenia-induced expansion of effector T cells after transfer into RAG1-deficient hosts (Extended Data Fig. 4c). Failure to persist in vivo did not seem to result from accelerated apoptosis, because the previously described high apoptotic rate of eT_{reg} cells¹¹

¹Center for Immunology and Inflammatory Diseases, Massachusetts General Hospital, Boston, MA, USA. ²Harvard Medical School, Boston, MA, USA. ³Division of Hematology/Oncology, Boston Children's Hospital, Boston, MA, USA. ⁴Center for Cancer Research, Massachusetts General Hospital, Boston, MA, USA. ⁵Department of Comparative Biomedicine and Food Science, University of Padua, Padova, Italy. ⁶These authors contributed equally: Mauro Di Pilato, Edward Y. Kim. *e-mail: mdipilato@mgh.harvard.edu; tmempel@mgh.harvard.edu

was not further enhanced in the absence of CARMA1 (Extended Data Fig. 4d). Lack of CARMA1 did not lead to an increase in the formation of FOXP3-negative 'exT_{reg}' cells (Extended Data Fig. 4e).

On the basis of global gene expression analyses, CARMA1-deficient eT_{reg} cells were equally dissimilar to control eT_{reg} cells as they were to control cT_{reg} cells, whereas CARMA1-deficient cT_{reg} cells were only moderately dissimilar to control cT_{reg} cells (Fig. 1i). In the latter, only 96 genes were differentially expressed, compared with 344 genes in eT_{reg} cells (Extended Data Fig. 5a and Supplementary Table 1). Based on differences between control cT_{reg} and eT_{reg} cells, we defined an 'eT_{reg} signature', which largely overlapped with a previously reported gene set^{12,13}. When examining these 689 genes, hemizygous *CARMA1*-deletion had only a moderate effect, whereas homozygous deletion induced major changes specifically in the eT_{reg} cell gene expression program (Fig. 1j and Extended Data Fig. 5b). Minor changes in the expression of the Bcl2 family of apoptotic regulator genes occurred during eT_{reg} cell differentiation, but CARMA1-deficient eT_{reg} cells did not deviate from this pattern apart from having less pronounced downregulation of BCL2 and BIM, confirming our observations on protein expression (Extended Data Fig. 6). Thus, a complete—and even a partial—loss of CARMA1 expression impairs eT_{reg} cell differentiation and persistence, but does not induce the cells to become pathogenic or convert to exT_{reg} cells under non-inflammatory conditions. However, in the context of incipient inflammation triggered by a global loss of the suppressive function of T_{reg} cells, CARMA1-deficient T_{reg} cells secrete IFN γ , which further accelerates inflammatory disease.

Failed thymic development of T_{reg} cells in the absence of CARMA1 results from disabled NF- κ B signalling and is restored through the expression of a constitutively active form of I κ B kinase 2 (referred to as IKK2ca)¹². Furthermore, the NF- κ B proteins REL (also known as c-Rel) and RELA (p65) have important roles in T_{reg} cell function^{13–15}, which suggests that failed activation of NF- κ B may primarily account for the effects of CARMA1-deletion in T_{reg} cells. However, the expression of IKK2ca in T_{reg} cells neither prolonged the lifespan of *F^{cre} × C1^{fl/fl}* mice, nor reduced the differentiation of effector T_{conv} cells (Extended Data Fig. 7a, b). Restoring NF- κ B activation did not restore differentiation of eT_{reg} cells, and did not limit the secretion of IFN γ , but only of TNF (Extended Data Fig. 7c, d). Therefore, although NF- κ B activation is evidently essential^{13,16}, additional CBM-complex effector functions are also crucial for maintaining T_{reg} cell function. The relevance of these additional functions will need to be investigated, but an initial examination of CARMA1-deficient T_{reg} cells from healthy *F^{cre/+} × C1^{fl/fl}* mice already revealed decreased expression and TCR-induced phosphorylation of FOXO1, possibly reflecting CARMA1- and TBK1-driven regulation of AKT activity¹⁷ (Extended Data Fig. 7e, f).

Considering the pro-inflammatory potential of CARMA1-deficient T_{reg} cells, we examined their tumour response. Subcutaneous implantation of the poorly immunogenic *Braf^{V600E} × Pten^{-/-}* melanoma D4M.3A¹⁸ into female *F^{cre/+} × C1^{fl/fl}* hosts amplified the effects of CARMA1-deficiency on T_{reg} cells, because the frequency not only of eT_{reg} cells but also of total T_{reg} cells was reduced in tumours and tumour-draining LNs (tDLNs) as a function of decreasing CARMA1 expression, accompanied also by a more pronounced reduction in FOXP3 expression (Extended Data Fig. 8a–d). Notably, we observed growth deceleration of D4M.3A melanoma, and of MC38 colon carcinoma, when half of the T_{reg} cells lacked one or both alleles of *CARMA1* (Fig. 2a and Extended Data Fig. 8e). Because a mere loss of function in only half of the T_{reg} cells is not predicted to cause loss of tumour tolerance¹⁹, this suggested active T_{reg}-cell-mediated anti-tumour activity. Indeed, a large fraction of completely or even partially CARMA1-deficient T_{reg} cells secreted both TNF and IFN γ in situ, whereas these effector cytokines were undetectable in tumour-infiltrating CD4⁺ and CD8⁺ T_{conv} cells (Fig. 2b, c). Importantly, no increase in cytokine secretion by T_{reg} cells was observed in tDLNs or in non-lymphoid tissues, such as skin or lung (Fig. 2d and Extended Data Fig. 8f, g). IFN γ expression in tumour tissue correlated with downregulation, but not

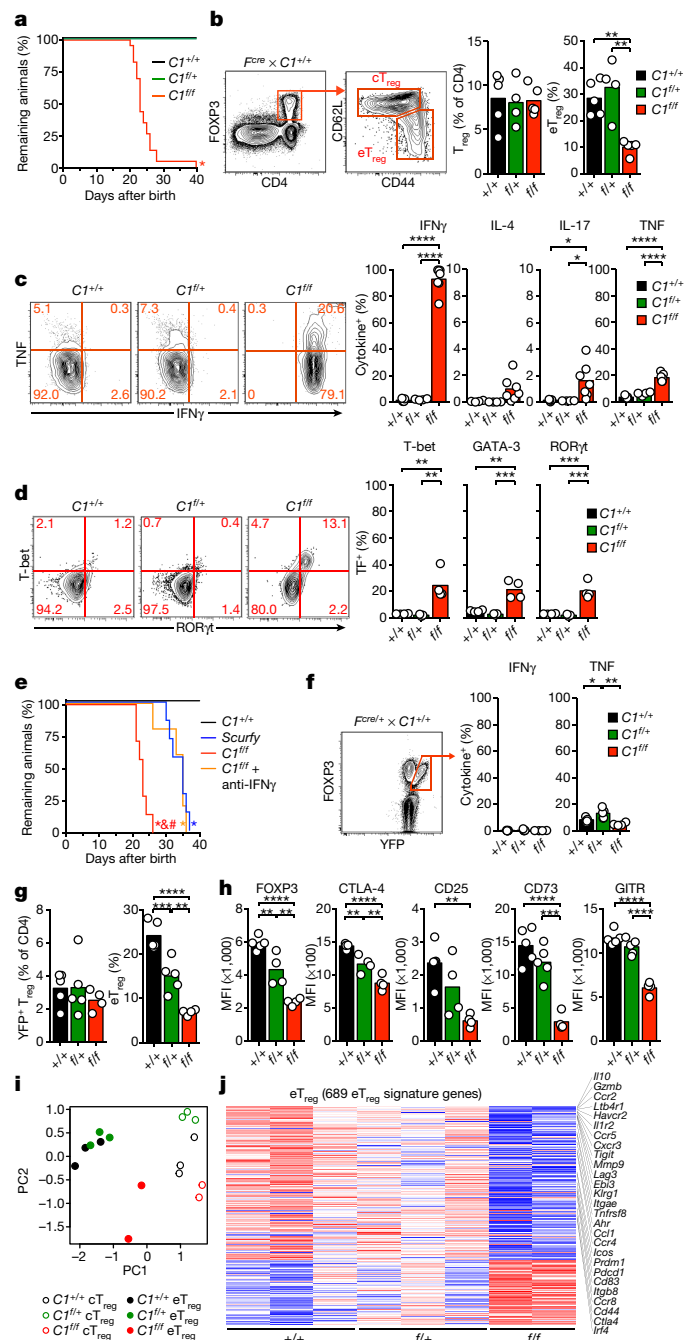


Fig. 1 | Loss of CARMA1 in T_{reg} cells is fatal, but reduced expression is sufficient to maintain immune tolerance. **a**, Survival of *F^{cre} × C1^{+/+}*, *C1^{fl/+}* and *C1^{fl/fl}* mice ($n = 8, 10$ and 20 per group, respectively). **b**, Frequency of T_{reg} cells among CD4⁺ T cells and of eT_{reg} cells among total T_{reg} cells in LNs. **c**, **d**, Expression of cytokines (**c**) and transcription factors (TF) (**d**) in LN T_{reg} cells after ex vivo stimulation. **e**, Survival of *F^{cre} × C1^{fl/fl}* mice treated with anti-IFN γ antibodies from day 14 of life, compared with *F^{cre} × C1^{+/+}* and *scurfy* mice. **f**, Cytokine expression of YFP⁺ T_{reg} cells from LNs of nine-week-old female heterozygous *F^{cre/+} × C1^{+/+}*, *C1^{fl/+}* and *C1^{fl/fl}* mice after ex vivo stimulation. **g**, Frequency of YFP⁺ T_{reg} cells among CD4⁺ T cells and of YFP⁺ eT_{reg} cells among total YFP⁺ T_{reg} cells in LNs. **h**, Expression of indicated proteins in YFP⁺ eT_{reg} cells from 9-week-old mice. Data in **b–h** represent two independent experiments with similar results. Data are mean and individual replicates. In **a** and **e**, * $P < 0.05$ versus wild type (+/+), & $P < 0.05$ versus *scurfy*, and # $P < 0.05$ versus anti-IFN γ (log-rank (Mantel–Cox) test). In all other panels, * $P < 0.05$, ** $P < 0.01$, *** $P < 0.001$, **** $P < 0.0001$ (one-way analysis of variance (ANOVA) with Tukey post hoc test). **i**, **j**, Bulk RNA sequencing analysis of YFP⁺ cT_{reg} and eT_{reg} cells from LNs of *F^{cre/+} × C1^{+/+}*, *C1^{fl/+}* and *C1^{fl/fl}* mice. **i**, Principal component (PC) analysis of transcriptomes. **j**, Scaled expression of eT_{reg} signature genes by eT_{reg} cells (defined by fold change > 2 and $P_{\text{adj}} < 0.01$ between *C1^{+/+}* cT_{reg} and *C1^{+/+}* eT_{reg} cells). Selected eT_{reg} cell genes are annotated.

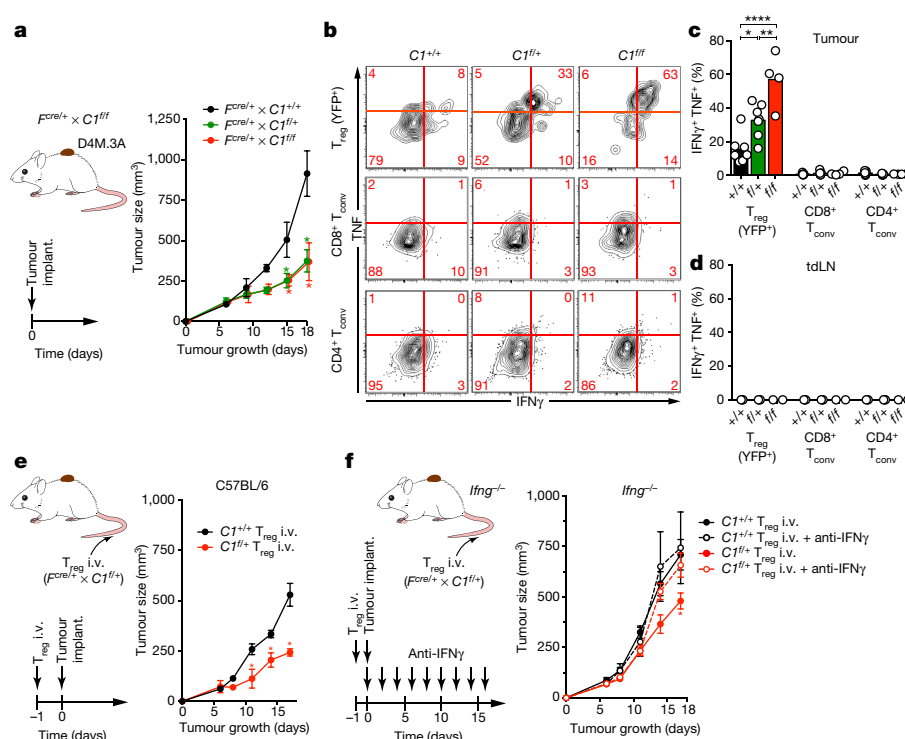


Fig. 2 | Reduced CARMA1 expression converts tumour-infiltrating T_{reg} cells into $IFN\gamma$ -secreting effector cells that dominantly control tumour growth. **a**, Female $F^{cre/+} \times C1^{+/+}$, $C1^{fl/+}$ and $C1^{fl/fl}$ mice were implanted with D4M.3A melanoma, and tumour growth was recorded. **b–d**, In situ expression in tumour tissue (**b**, **c**) or tdLNs (**d**) of effector cytokines in YFP^{+} T_{reg} cells lacking one or both alleles of CARMA1 as well as in $CD4^{+}$ and $CD8^{+}$ T_{conv} cells 18 days after tumour implantation. **e**, **f**, One million YFP^{+} T_{reg} cells from $F^{cre/+} \times C1^{fl/+}$ or $C1^{+/+}$ mice were

injected intravenously (i.v.) into either C57BL/6 (**e**) or $IFN\gamma$ -deficient (**f**) hosts, which were implanted with D4M.3A melanoma the next day, and tumour growth was recorded. Some $IFN\gamma$ -deficient hosts were treated with neutralizing anti- $IFN\gamma$ antibody. Data represent two independent replicates with similar results. Data are mean and either individual replicates (**c**, **d**) or s.e.m. (**a**, **e**, **f**). * $P < 0.05$, ** $P < 0.01$, **** $P < 0.0001$ (two-way ANOVA with Bonferroni post hoc test in **a**, **f**; one-way ANOVA with Tukey post hoc test in **c**, **d**; two-tailed Student's t -test in **e**).

loss of FOXP3 in both partially and fully CARMA1-deficient T_{reg} cells (Extended Data Fig. 8h). Notably, destabilization of control T_{reg} cells by $IFN\gamma$ -producing T_{reg} cells, as described in other settings²⁰, did not occur because no increase in cytokine expression was detectable in YFP^{+} CARMA1-sufficient T_{reg} cells in the same tumours (not shown). Neutralization of $IFN\gamma$ fully restored tumour growth in $F^{cre/+} \times C1^{fl/fl}$ mice (Extended Data Fig. 8i), which suggests a crucial role for this cytokine in T_{reg} -cell-mediated anti-tumour immunity. However, $IFN\gamma$ may also derive from other cellular sources after T_{reg} cell destabilization. To test the role of T_{reg} -cell-produced $IFN\gamma$ specifically, we transferred T_{reg} cells with reduced expression of CARMA1 into tumour-bearing

C57BL/6 or $Ifng^{-/-}$ mice. In both hosts, T_{reg} cells stunted tumour growth similarly, but not when $IFN\gamma$ was neutralized, which indicates that T_{reg} -cell-derived $IFN\gamma$ is both necessary and sufficient for anti-tumour effects (Fig. 2e, f and Extended Data Fig. 8j–m). Therefore, although neither partially nor fully CARMA1-deficient T_{reg} cells cause inflammation in healthy mice, both are selectively destabilized in tumour tissue and secrete $IFN\gamma$ to decelerate tumour growth.

Expression of IKK2ca restored the frequencies of total T_{reg} and eT_{reg} cells in tdLNs, but not in tumour tissue (Extended Data Fig. 9a). It did not restore FOXP3 expression, only partially reduced TNF and $IFN\gamma$ co-expression by tumour-infiltrating CARMA1-deficient

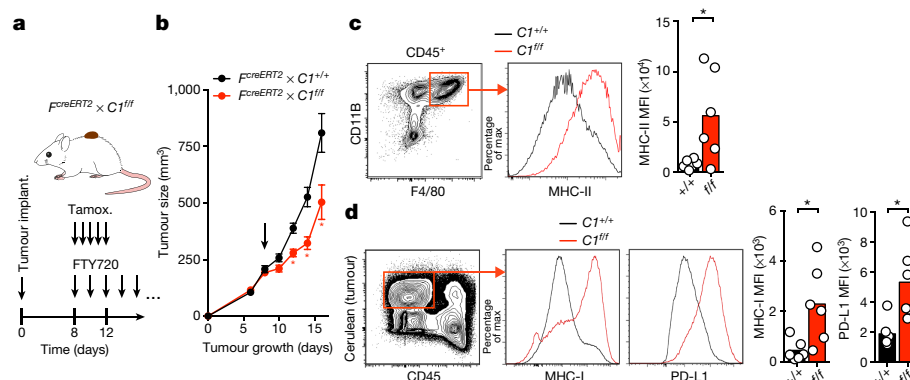


Fig. 3 | CARMA1-deleted T_{reg} cells rapidly induce tumour inflammation but also adaptive immune resistance. **a**, **b**, D4M.3A melanoma growth in $F^{creERT2} \times C1^{+/+}$ and $C1^{fl/fl}$ mice treated with tamoxifen from days 8–12 as well as with FTY720 starting the same day until the end of the experiment. Arrow in **b** indicates the start of treatment. **c**, **d**, MHC-II surface expression on $F4/80^{+}$ tumour macrophages (**c**), and MHC-I and PD-L1

expression on D4M.3A tumour cells (expressing blue-fluorescent H2B-Cerulean) (**d**) three days after the initiation of tamoxifen treatment. MFI, mean fluorescence intensity. Data represent two independent replicates with similar results. Data are mean and individual replicates (**c**, **d**) or s.e.m. (**b**). * $P < 0.05$ (two-tailed Student's t -test).

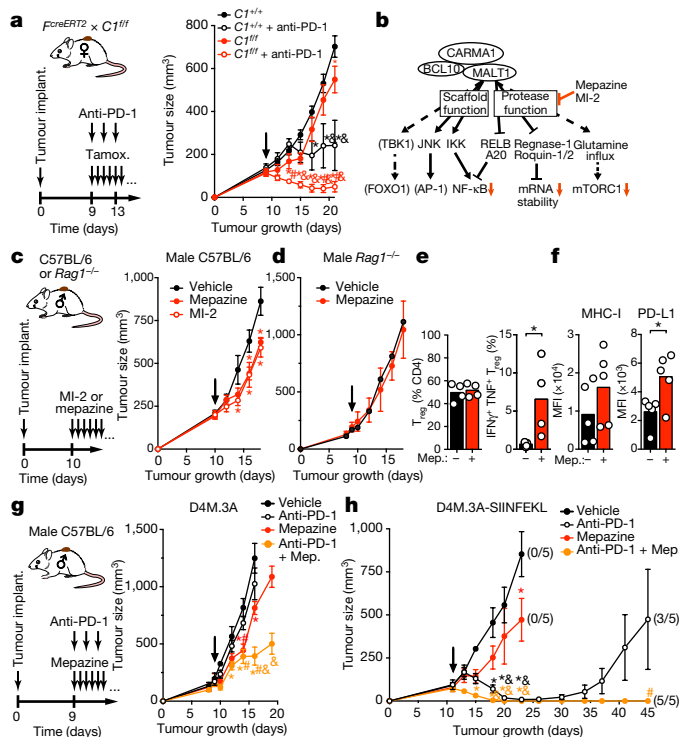


Fig. 4 | CARMA1 deletion in T_{reg} cells and pharmacological inhibition of MALT1 protease synergize with anti-PD-1 ICT. **a**, Female $F^{creERT2} \times C1^{fl/fl}$ and $C1^{fl/fl}$ mice were implanted with D4M.3A melanoma, and treated with tamoxifen starting on day 9 until the end of the experiment, as well as with three doses of the anti-PD-1-antibody 29F.1A12 or isotype control, and tumour growth was recorded. **b**, CBM complex effector pathways and predicted effects (red arrows) of the MALT1 protease inhibitors mepazine and MI-2. **c, d**, D4M.3A tumour growth in C57BL/6 (c) or RAG1-deficient (d) hosts treated with MALT1 inhibitors (MI-2 or mepazine). Dimethylsulfoxide (DMSO) was used as a vehicle control. **e, f**, Effects of mepazine treatment for three days on intratumoral T_{reg} cell frequency and their in situ expression of effector cytokines (e), and on the expression of MHC-I and PD-L1 on tumour cells (f). **g, h**, Synergistic control of tumours by combined anti-PD-1 and mepazine treatment of poorly immunogenic D4M.3A (g) and immunogenic D4M.3A-SIINFEKL (h) tumours in male C57BL/6 hosts. Numbers in parentheses indicate fraction of mice without relapse for more than 12 months after discontinuation of treatment. Data in a, c–f represent two independent replicates with similar results. Data are mean and individual replicates (e, f) or s.e.m. (a, c, d, g, h). Arrows in tumour growth charts indicate the start of treatment. In a, $*P < 0.05$ versus $C1^{+/+}$, $\#P < 0.05$ versus $C1^{+/+} + \text{anti-PD-1}$, and $\&P < 0.05$ versus $C1^{fl/fl}$. In g and h, $*P < 0.05$ versus vehicle (DMSO), $\#P < 0.05$ versus anti-PD-1, and $\&P < 0.05$ versus mepazine, respectively. In e, $*P < 0.05$ (two-way ANOVA with Bonferroni post hoc test in a, c, g, h; two-tailed Student's *t*-test in d–f).

T_{reg} cells, and did not prevent their anti-tumour activity (Extended Data Fig. 9b–d), which emphasizes the importance of CBM-complex effector functions other than NF- κ B activation¹⁶ in stabilizing tumour-reactive T_{reg} cells.

To examine whether CARMA1 deletion acutely destabilizes intratumoral T_{reg} cells, we generated $Foxp3^{GFP-creERT2} \times CARMA1^{fl/fl}$ (hereafter termed $F^{creERT2} \times C1^{fl/fl}$) mice and treated these with tamoxifen to trigger Cre-mediated CARMA1 deletion when tumours were already established (Fig. 3a and Extended Data Fig. 9e). To prevent subsequent recruitment of additional T_{reg} cells from tdLNs, we concurrently blocked lymphocyte tissue egress using the functional S1P receptor antagonist FTY720, as previously described⁴. Within two days of treatment, tumour growth decelerated (Fig. 3b). A similarly rapid, albeit slightly less pronounced, growth effect as well as increased secretion of effector cytokines by T_{reg} cells resulted from deletion of CARMA1 in only half of the T_{reg} cells (Extended Data Fig. 9f, g). Intratumoral

destabilization of T_{reg} cells was accompanied by pronounced induction of macrophage expression of cell-surface major histocompatibility complex class II (MHC-II) molecules, both after constitutive or acute deletion of one or both alleles of *CARMA1* in T_{reg} cells (Fig. 3c and Extended Data Fig. 9h). Furthermore, the expression of MHC-I molecules on tumour cells increased, predictably sensitizing them to cytotoxic-T-lymphocyte (CTL)-mediated lysis (Fig. 3d). Although T_{reg} cell-derived IFN γ thus caused widespread tumour inflammation, it also triggered tumour cell-expression of PD-L1, a ligand for the T cell inhibitory receptor PD-1, which suggests that concurrent induction of adaptive immune resistance³ limited improved tumour control resulting from enhanced anti-tumour immune effector functions (Fig. 3d).

Considering the induction of PD-L1 on tumour cells, we hypothesized that antibody-mediated blockade of PD-1 may synergize with the anti-tumour effects of IFN γ -secreting T_{reg} cells. Indeed, treatment with anti-PD-1 antibody simultaneously with CARMA1 deletion in T_{reg} cells enabled much more rapid and consistent control of D4M.3A melanoma than either treatment alone (Fig. 4a). Targeting the CBM complex in T_{reg} cells may thus be highly effective at enhancing the potency of immune checkpoint therapy (ICT) in patients with cancer.

Although pharmacological inhibitors of the scaffold protein CARMA1 are, to our knowledge, currently not available, inhibitors of MALT1 paracaspase are predicted to attenuate the majority of CBM-complex-dependent effector pathways (Fig. 4b). Indeed, similar to CARMA1-deficient mice, T_{reg} cells are virtually absent in mice that express mutant MALT1 proteins that lack paracaspase activity (replicating continual and complete pharmacological inhibition)^{21–23}. We therefore tested the allosteric MALT1 inhibitor mepazine^{24,25} and the catalytic site binder MI-2²⁶ for activity against solid tumours. Both inhibitors produced a similar deceleration in melanoma growth to that observed after deletion of CARMA1 in T_{reg} cells (Fig. 4c), even when CD8⁺ T cells were depleted (Extended Data Fig. 9i). Systemic inhibition of MALT1 will also target cells other than T_{reg} cells, including melanoma cells²⁷. However, no effect on tumour growth occurred in RAG1-deficient mice that lack lymphocytes (Fig. 4d). Inhibition of MALT1 did not synergize with deletion of CARMA1 in T_{reg} cells, which suggests that the anti-tumour activity of MALT1 does not result from effects other than attenuated CBM complex function in T_{reg} cells (Extended Data Fig. 9j). Because MALT1 inhibition is predicted to attenuate, and not enhance lymphocyte effector functions²⁸, we conclude that its effect on tumour growth is probably mediated through destabilization of T_{reg} cells. Similar to T_{reg} -cell-specific deletion of CARMA1, treatment with mepazine caused a rapid, albeit less pronounced, induction of TNF and IFN γ expression by tumour-infiltrating T_{reg} cells (Fig. 4e). Short-term in vitro treatment of T_{reg} cells triggered only a minor reduction of FOXP3, GITR and CTLA-4 expression (Extended Data Fig. 10a) and did not induce IFN γ secretion (data not shown), which indicates that the latter occurs only under the conditions of the tumour microenvironment. Accordingly, mepazine caused upregulation of the expression of PD-L1 and MHC-I molecules on tumour cells in vivo (Fig. 4f) and induction of *Ifng* and a wide range of IFN γ -regulated genes indicative of both T_H1 inflammation and adaptive immune resistance in tumour tissue (Extended Data Fig. 10b). In contrast to constitutive deletion of CARMA1, short-term inhibition of MALT1 did not reduce the frequency of T_{reg} cells, and the expression of T_{reg} -cell-associated genes in tumour tissue was not reduced (Fig. 4e and Extended Data Fig. 10c). Nevertheless, in addition to overall enhanced infiltration of immune cells, treatment with mepazine specifically increased the frequencies of CTL and natural killer cells in tumour tissue (Extended Data Fig. 10d–h).

A high tumour mutational load favours response to ICT in patients with cancer^{29,30}, and a low mutational burden remains a major challenge that limits the success of this form of immunotherapy to some cancer types and to a minority of patients. Accordingly, D4M.3A melanoma, which carries a negligible mutational load relative to the C57BL/6J reference exome (D. E. Fisher, personal communication),

is completely resistant to anti-PD-1 monotherapy in male hosts (Fig. 4g), in contrast to female hosts, in which Y-antigen-expressing male D4M.3A tumours showed a partial response (Fig. 4a). Concurrent MALT1 inhibition, however, synergized with anti-PD-1 treatment, and arrested tumour growth even in male hosts (Fig. 4g). Anti-PD-1 treatment did not further increase T_{reg} cell expression of $IFN\gamma$, indicating that PD-1 did not restrict the pro-inflammatory function of destabilized T_{reg} cells (Extended Data Fig. 10i). Furthermore, when we raised the immunogenicity of D4M.3A tumours by expressing the chicken ovalbumin-derived SIINFEKL epitope as a surrogate mutational neoantigen, we observed an initial response to anti-PD-1 monotherapy, but 40% of tumours relapsed. A combination of anti-PD-1 antibodies with mepazine, however, produced accelerated rejection and prevented relapse (Fig. 4h). Finally, to explore the effects of MALT1 inhibition on other cancer types, we treated mice implanted with MC38 colon carcinoma. Although anti-PD-1 monotherapy had only a moderate effect on late-stage tumours, combination with mepazine enabled profound tumour control and relapse-free rejection in most mice (Extended Data Fig. 10j). Hence, systemic inhibition of MALT1 inflames the tumour environment and renders poorly immunogenic tumours responsive to anti-PD-1 therapy while enhancing responses of immunogenic tumours and minimizing the frequency of relapse, a common problem in clinical ICT³¹.

We propose that inhibition of MALT1 protease or of other CBM complex functions could be a useful therapeutic strategy to elicit an intratumoral T_H1 autoimmune reaction mediated by locally destabilized, preferentially self-reactive T_{reg} cells. Pro-inflammatory effects of destabilized T_{reg} cells seem to outweigh any potential attenuation of immune effector cell activities through MALT1 inhibition. Owing to its selectivity for intratumoral T_{reg} cells, this treatment may increase the fraction of patients with cancer who respond to PD-1/PD-L1-targeted ICT or other forms of immunotherapy, without inducing systemic autoimmune toxicity.

Online content

Any methods, additional references, Nature Research reporting summaries, source data, statements of data availability and associated accession codes are available at <https://doi.org/10.1038/s41586-019-1215-2>.

Received: 15 December 2017; Accepted: 17 April 2019;

Published online 15 May 2019.

1. Savage, P. A., Leventhal, D. S. & Malchow, S. Shaping the repertoire of tumor-infiltrating effector and regulatory T cells. *Immunol. Rev.* **259**, 245–258 (2014).
2. Mellman, I., Coukos, G. & Dranoff, G. Cancer immunotherapy comes of age. *Nature* **480**, 480–489 (2011).
3. Spranger, S. et al. Up-regulation of PD-L1, IDO, and T_{reg} s in the melanoma tumor microenvironment is driven by CD8⁺ T cells. *Sci. Transl. Med.* **5**, 200ra116 (2013).
4. Bauer, C. A. et al. Dynamic T_{reg} interactions with intratumoral APCs promote local CTL dysfunction. *J. Clin. Invest.* **124**, 2425–2440 (2014).
5. Meiningner, I. & Krappmann, D. Lymphocyte signaling and activation by the CARMA1-BCL10-MALT1 signalosome. *Biol. Chem.* **397**, 1315–1333 (2016).
6. Medoff, B. D. et al. Differential requirement for CARMA1 in agonist-selected T-cell development. *Eur. J. Immunol.* **39**, 78–84 (2009).
7. Molinero, L. L. et al. CARMA1 controls an early checkpoint in the thymic development of FoxP3⁺ regulatory T cells. *J. Immunol.* **182**, 6736–6743 (2009).
8. Barnes, M. J. et al. Commitment to the regulatory T cell lineage requires CARMA1 in the thymus but not in the periphery. *PLoS Biol.* **7**, e1000051 (2009).
9. Brüstle, A. et al. MALT1 is an intrinsic regulator of regulatory T cells. *Cell Death Differ.* **24**, 1214–1223 (2017).
10. Schmidt-Suppran, M. et al. Differential dependence of CD4⁺CD25⁺ regulatory and natural killer-like T cells on signals leading to NF- κ B activation. *Proc. Natl Acad. Sci. USA* **101**, 4566–4571 (2004).
11. Smigielski, K. S. et al. CCR7 provides localized access to IL-2 and defines homeostatically distinct regulatory T cell subsets. *J. Exp. Med.* **211**, 121–136 (2014).
12. Long, M., Park, S.-G., Strickland, I., Hayden, M. S. & Ghosh, S. Nuclear factor- κ B modulates regulatory T cell development by directly regulating expression of Foxp3 transcription factor. *Immunity* **31**, 921–931 (2009).
13. Oh, H. et al. An NF- κ B transcription-factor-dependent lineage-specific transcriptional program promotes regulatory T cell identity and function. *Immunity* **47**, 450–465.e5 (2017).

14. Vasanthakumar, A. et al. The TNF receptor superfamily-NF- κ B axis is critical to maintain effector regulatory T cells in lymphoid and non-lymphoid tissues. *Cell Rep.* **20**, 2906–2920 (2017).
15. Messina, N. et al. The NF- κ B transcription factor RelA is required for the tolerogenic function of Foxp3⁺ regulatory T cells. *J. Autoimmun.* **70**, 52–62 (2016).
16. Grinberg-Bleyer, Y. et al. NF- κ B c-Rel is crucial for the regulatory T cell immune checkpoint in cancer. *Cell* **170**, 1096–1108.e13 (2017).
17. Yu, J. et al. Regulation of T-cell activation and migration by the kinase TBK1 during neuroinflammation. *Nat. Commun.* **6**, 6074 (2015).
18. Jenkins, M. H. et al. Multiple murine BRAF^{V600E} melanoma cell lines with sensitivity to PLX4032. *Pigment Cell Melanoma Res.* **27**, 495–501 (2014).
19. Pierson, W. et al. Antiapoptotic Mcl-1 is critical for the survival and niche-filling capacity of Foxp3⁺ regulatory T cells. *Nat. Immunol.* **14**, 959–965 (2013).
20. Overacre-Delgoffe, A. E. et al. Interferon- γ drives T_{reg} fragility to promote anti-tumor immunity. *Cell* **169**, 1130–1141.e11 (2017).
21. Gewies, A. et al. Uncoupling Malt1 threshold function from paracaspase activity results in destructive autoimmune inflammation. *Cell Reports* **9**, 1292–1305 (2014).
22. Jaworski, M. et al. Malt1 protease inactivation efficiently dampens immune responses but causes spontaneous autoimmunity. *EMBO J.* **33**, 2765–2781 (2014).
23. Bornancin, F. et al. Deficiency of MALT1 paracaspase activity results in unbalanced regulatory and effector T and B cell responses leading to multiorgan inflammation. *J. Immunol.* **194**, 3723–3734 (2015).
24. Nagel, D. et al. Pharmacologic inhibition of MALT1 protease by phenothiazines as a therapeutic approach for the treatment of aggressive ABC-DLBCL. *Cancer Cell* **22**, 825–837 (2012).
25. Schlauderer, F. et al. Structural analysis of phenothiazine derivatives as allosteric inhibitors of the MALT1 paracaspase. *Angew. Chem. Int. Edn Engl.* **52**, 10384–10387 (2013).
26. Fontan, L. et al. MALT1 small molecule inhibitors specifically suppress ABC-DLBCL *in vitro* and *in vivo*. *Cancer Cell* **22**, 812–824 (2012).
27. Wang, Y. et al. MALT1 promotes melanoma progression through JNK/c-Jun signaling. *Oncogenesis* **6**, e365 (2017).
28. Thome, M., Charton, J. E., Pelzer, C. & Hailfinger, S. Antigen receptor signaling to NF- κ B via CARMA1, BCL10, and MALT1. *Cold Spring Harb. Perspect. Biol.* **2**, a003004–a003004 (2010).
29. Le, D. T. et al. PD-1 blockade in tumors with mismatch-repair deficiency. *N. Engl. J. Med.* **372**, 2509–2520 (2015).
30. Rizvi, N. A. et al. Cancer immunology. Mutational landscape determines sensitivity to PD-1 blockade in non-small cell lung cancer. *Science* **348**, 124–128 (2015).
31. Zaretsky, J. M. et al. Mutations associated with acquired resistance to PD-1 blockade in melanoma. *N. Engl. J. Med.* **375**, 819–829 (2016).

Acknowledgements We thank the MGH Pathology Flow Cytometry Core and N. Ali-Akbar for technical assistance. This study was funded by an EMBO fellowship (ALTF534-2015) and a Marie Curie Global Fellowship (750973) (M.D.P.), DFG Fellowships (PR 1652/1-1 to J.N.P. and US 116/2-1 to S.M.U.), NIH T32 CA207021 (V.M.), a Sara Elizabeth O'Brien Fellowship (F.M.), and Melanoma Research Alliance Senior Investigator Award MRA-348693, NIH AI123349, and the Bob and Laura Reynolds MGH Research Scholar Award (T.R.M.).

Reviewer information Nature thanks Shimon Sakaguchi and the other anonymous reviewer(s) for their contribution to the peer review of this work.

Author contributions M.D.P. initiated, designed, performed and analysed the experiments, and wrote the manuscript. E.Y.K. initiated the project, designed and performed experiments, V.Z. performed histological analyses, S.M.U. performed autoantibody assays, V.M. and F.M. performed T_{reg} cell analyses in lung and skin. F.M. performed *in vitro* T_{reg} suppression assay. E.C. generated tumour cell lines. M.N.N. and A.-C.V. performed RNA sequencing analyses, B.D.M. provided genetic mouse models, D.S. designed and performed RT-qPCR assay, B.L.C., S.M., J.N.P., R.D.W. and M.L. performed tumour growth studies and survival studies, T.R.M. conceived the study, supervised the project, designed experiments, and wrote the manuscript.

Competing interests M.D.P. and T.R.M. have filed a patent application (PCT/US2018/067856) related to the use of MALT1 inhibitors. T.R.M. is a co-founder of Monopteros Therapeutics. All other authors declare no competing interests.

Additional information

Extended data is available for this paper at <https://doi.org/10.1038/s41586-019-1215-2>.

Supplementary information is available for this paper at <https://doi.org/10.1038/s41586-019-1215-2>.

Reprints and permissions information is available at <http://www.nature.com/reprints>.

Correspondence and requests for materials should be addressed to M.D.P. or T.R.M.

Publisher's note: Springer Nature remains neutral with regard to jurisdictional claims in published maps and institutional affiliations.

© The Author(s), under exclusive licence to Springer Nature Limited 2019

METHODS

Mice. *Foxp3*^{YFP-cre} (ref. 32), *Foxp3*^{GFP-creERT2} (ref. 33), *ROSA26-stop^{flf}-YFP* (ref. 34), *ROSA26-stop^{flf}-IKK2ca* (ref. 35), *Irfng*^{-/-36}, *B6-scurfy* (ref. 37) and C57BL/6J mice were purchased from Jackson Laboratories. R. J. Xavier and J. J. Moon provided *CARMA1*^{flf} (ref. 38) and *Rag1*^{-/-} mice, respectively. Animals were housed in specific-pathogen-free facilities at the Massachusetts General Hospital (MGH) and all experimental studies were approved and performed in accordance with guidelines and regulations implemented by the MGH Institutional Animal Care and Use Committee (IACUC). For survival studies, the age of mice at euthanasia mandated by a moribund state of health was recorded in Kaplan–Meyer plots.

Tumour cell lines. The *Braf*^{V600E} × *Pten*^{-/-} melanoma cell line D4M.3A (ref. 18) was provided by D. E. Fisher. For some experiments, D4M.3A cells were lentivirally transduced to express a blue fluorescent histone H2B–Cerulean fusion protein (D4M.3A–H2B–Cerulean), as previously described³⁹, to facilitate detection by flow cytometry. To generate D4M.3A–SIINFEKL tumours expressing the chicken ovalbumin-derived H-2K^b-restricted SIINFEKL peptide, we transduced D4M.3A cells with a VSV-G pseudotyped pHAGE-EF1α lentiviral vector engineered to express a fusion of histone H2B and Cerulean separated by two copies of the SIINFEKL minigene and its native flanking sequences in the ovalbumin protein to facilitate processing for antigen presentation. The colon adenocarcinoma cell line MC38⁴⁰ was obtained from A. D. Luster. All tumour lines were grown in DMEM with 10% fetal calf serum (FCS) and used for experiments when in exponential growth phase.

Tumour growth studies and treatments. One million D4M.3A, D4M.3A–H2B–Cerulean, D4M.3A–SIINFEKL or MC38 tumour cells were injected subcutaneously in 100 µl HBSS without Ca²⁺ into the flanks of mice. Wherever possible, animals were randomized into treatment groups. Tumour volumes were measured every second to third day after the start of treatments and calculated as $V = (\text{length} \times \text{width}^2)/2$.

Tamoxifen (1 mg per mouse in 100 µl of a 9:1 mixture of olive oil and ethanol) was injected intraperitoneally daily as indicated. FTY720 (1 mg kg⁻¹ bodyweight) in 150 µl H₂O was injected intraperitoneally every other day until the end of the experiment. Anti-IFNγ antibody (500 µg per mouse; clone XMG1.2) was injected intraperitoneally on day 14 after birth or on the day of tumour implantation and then every other day thereafter until the end of the experiment. Anti-PD-1 (200 µg; clone 29F.1A12) or rat IgG2a isotype control (200 µg; clone 2A3) was injected intraperitoneally three times in 100 µl PBS every other day at the indicated time points. Anti-CD8α (150 µg; clone YTS169.4) was injected in 100 µl PBS every other day from the indicated time point until the end of the experiment. Mepazine (16 mg kg⁻¹ bodyweight in 5% dimethylsulfoxide (DMSO)) or MI-2 (20 mg kg⁻¹ in 5% DMSO in purified H₂O) was injected intraperitoneally daily starting at the indicated time points until the end of the experiment, unless indicated otherwise. For adoptive T_{reg} cell transfer studies, CD4⁺ YFP⁺ T_{reg} cells were purified to more than 95% purity through magnetic-activated cell sorting (Miltenyi) from LNs and spleen of *F^{cre}* × *C1^{fl/+}* or *C1^{fl/+}* mice and 10⁶ cells per mouse were injected intravenously into the tail vein the day before tumour implantation.

Preparation of single-cell suspensions, antibody staining and flow cytometry. Heparinized peripheral blood collected through sub-mandibular vein puncture was treated with ACK red blood cell lysis buffer. LNs and spleens were passed through 40-µm cell strainers, followed by red blood cell lysis (spleens only). Tumours and lung tissue were minced into small fragments and treated with 1.5 mg ml⁻¹ collagenase IV and 50 U ml⁻¹ DNase I for 30 min at 37 °C under agitation. Skin tissue was digested in medium containing 2% FCS, 10 mM HEPES, 0.5 mg ml⁻¹ hyaluronidase, 1.5 mg ml⁻¹ collagenase IV, and 50 U ml⁻¹ DNase I for 45 min at 37 °C under agitation. Residual tissue fragments were mechanically dissociated.

Cell surface proteins were stained for 20 min at 4 °C with the following antibodies against: CD11b (M1/70), CD120b/TNFR2 (polyclonal Armenian hamster IgG), CD274/PD-L1 (10F9G2), CD357/GITR (DTA-1), CD4 (GK1.5), CD45 (30-F11), CD62L (MEL-14), CD73 (TY11.8), CD8α (53-6.7), CD90.2 (30-H12), F4/80 (BM8), H-2K^b (AF6-88.5), -I-A/I-E (M5/114.15.2), Ly-6C (HK1.4), Ly-6G (1A8), CD45R/B220 (RA3-6B2), CD64 (FcγRI) (X54-5/7.1), CD11c (N418), CD103 (2E7), NK-1.1 (PK136), CD335 (NKP46) (29A1.4), CD3 (17A2), CD19 (1D3/CD19), CD45RB (16A), and CD44 (IM7) (BioLegend), CD11c (HL3) and CD25 (PC61.5) (eBioscience).

Intracellular and nuclear proteins were stained for 60 min at room temperature after permeabilization and fixation (Mouse regulatory T cell staining Kit; eBioscience) using antibodies against: CD152/CTLA-4 (UC10-4B9), TNF (MP6-XT22), IL-4 (11B11), IL-17A (TC11-18H10.1), IFNγ (XMG1.2), T-bet (4B10), and Ki67 (16A8) (BioLegend), BIM (C34C5), CARD11/CARMA1 (1D12) (Cell Signaling), FOXP3 (FJK-16 s, eBioscience), GATA-3 (L50-823) and Ki67 (B56) (BD Biosciences), RORγt (AFKJS-9) and GFP (rabbit polyclonal) (Invitrogen). Polyclonal goat anti-rabbit Ig (H+L) secondary antibody (Life Technologies) was used to reveal primary anti-CARMA1 staining.

Preceding antibody staining, dead cells were stained using the fixable viability violet dye Zombie Red (Biolegend) for 15 min at room temperature, followed by blocking of Fc receptors with TruStain FcX (Biolegend) for 20 min at 4 °C. Cells were analysed on LSR II, LSRFortessa or LSRFortessa X-20 flow cytometers (BD Biosciences), and data were analysed with FlowJo software v.9.9.5.

Phospho-protein analysis. LN single-cell suspensions were stained using the fixable viability dye ZombieRed (Biolegend) for 15 min at room temperature, and added for 30 min at 37 °C to tissue culture plates pre-coated overnight with anti-CD3ε (clone 145-2C11) and anti-CD28 (clone 37.51) antibodies (at 10 µg ml⁻¹ of each antibody), or to uncoated control plates. Samples were then fixed in 4% paraformaldehyde (PFA) for 10 min at room temperature, and permeabilized for 20 min through dropwise addition of 1 ml ice-cold methanol. Cells were then stained for CD90.2 (30-H12), CD4 (GK1.5), CD8α (53-6.7), CD44 (IM7) (BioLegend), Foxp3 (FJK-16 s, eBioscience), pFoxo1 (Thr24)/Foxo3a (Thr32), p-c-Jun (Ser73) (D47G9) (Cell Signaling) and GFP (rabbit polyclonal Ab) (Invitrogen).

Analysis of in situ and ex vivo stimulated cytokine secretion. To detect in situ cytokine secretion, mice were slowly injected intravenously with 500 µg of brefeldin A in 250 µl PBS 6 h before euthanasia and intracellular cytokine staining.

To detect cytokine secretion in T cells upon ex vivo re-stimulation, single-cell suspensions from tumours and LNs were resuspended in RPMI 1640 with 10% FCS and added to anti-CD3 (clone 145-2C11)/anti-CD28 (clone 37.51) antibody-coated (overnight at 10 µg ml⁻¹ antibody) tissue culture plates for 8 h at 37 °C in the presence of 1 µg ml⁻¹ Golgiplug and Monensin (both from Biolegend) and cells processed for intracellular cytokine staining.

Analysis of exT_{reg} cells. CD4⁺ YFP^{bright} cells were first purified by FACS from LNs and spleens of *Foxp3*^{YFP-cre/+} × *CARMA1*^{flf} (or *fl/+* or *+/+*) × *ROSA26*^{YFP} mice and stained for FOXP3 expression for flow cytometry analysis, as described above.

In vivo and in vitro suppression. For in vivo suppression studies, 3 × 10⁵ Miltenyi (negative selection) enriched CD4⁺ and FACS sorted (>98% purity) CD45RB^{high} YFP⁻ cells from LNs and spleens of *Foxp3*^{YFP-cre/cre} mice were intravenously injected into the tail vein of *Rag1*^{-/-} mice with or without 1 × 10⁵ Miltenyi (negative selection) enriched CD4⁺ and FACS sorted (>98% purity) YFP^{bright} T_{reg} cells from LNs and spleens of *Foxp3*^{YFP-cre/+} × *CARMA1*^{flf} (or *CARMA1*^{fl/+} or *CARMA1*^{+/+}) × *ROSA26*^{YFP} mice.

For in vitro suppression studies, 1 × 10⁴ FACS-sorted (>98% purity) CD4⁺ YFP⁻ conventional T cells from LNs and spleens of *Foxp3*^{YFP-cre/cre} mice were labelled with 5 µM CellTrace Violet and stimulated with 250 ng ml⁻¹ of anti-CD3 monoclonal antibody (145-2c11, Biolegend) in presence of 2.5 × 10⁴ T-cell depleted splenocytes and different concentrations (from 1:1 to 1:16) of Miltenyi (negative selection) enriched CD4⁺ and FACS sorted (>98% purity) YFP^{bright} T_{reg} cells from LNs and spleens of *Foxp3*^{YFP-cre/+} × *CARMA1*^{flf} (or *CARMA1*^{fl/+} or *CARMA1*^{+/+}) × *ROSA26-stop^{flf}-YFP* mice. CD4⁺ YFP⁻ conventional T cell proliferation was read out after 72 h, as previously described⁴¹. In brief, percentage of suppression was scaled from 0 (proliferation of conventional T cell in absence of T_{reg} cells) to 100 (complete absence of proliferation).

In vitro apoptosis. Enriched CD4⁺ and FACS-purified (>99% purity) YFP^{bright} T_{reg} cells from LNs of *Foxp3*^{YFP-cre/+} × *CARMA1*^{flf} (or *CARMA1*^{+/+}) × *ROSA26-stop^{flf}-YFP* mice were added for 6 and 18 h at 37 °C to tissue culture plates pre-coated overnight with anti-CD3ε (clone 145-2C11) and anti-CD28 (clone 37.51) antibodies (at 10 µg ml⁻¹ of each antibody). Viability of CD44^{low}CD62L⁺ cT_{reg} and CD44^{high}CD62L⁻ eT_{reg} cells was then read out by annexin V and Zombie Red staining (Biolegend).

RNA sequencing studies: sample collection. CD4⁺ T cells from LNs and spleens of *F^{cre}* × *C1^{+/+}*, *C1^{fl/+}* or *C1^{fl/fl}* mice were pre-enriched by immunomagnetic cell sorting (Miltenyi negative selection) and then 5 × 10³ YFP⁺CD4⁺CD44^{low}CD62L⁺ cT_{reg} cells per animal and the same number of YFP⁺CD4⁺CD44^{high}CD62L⁻ eT_{reg} cells were sorted to >99% purity directly into 10 µl lysis buffer consisting of TCL buffer (Qiagen) and 1% of β-mercaptoethanol. Samples were then flash-frozen and kept at -80 °C before further processing following a modified version of the Smart-Seq2 protocol^{11,12,14}, as described below. A total of 18 samples was collected, but 2 samples were discarded for technical reasons.

Reverse transcription. Samples were thawed on ice for 2 min, and then centrifuged at 2,500 rpm at 4 °C for 1 min and the RNA concentration normalized. RNA (1.9 µl per sample) was moved to a full-skrat 96-well plate (Eppendorf). Each sample was then mixed with 1 µl 10 µM RT primer 5'-AAGCAGTGGTATCAACGCAGAGTACTTTTTTTTTTTTTTTTTTTTTTTT TTTTTTTVN-3' (IDT), 1 µl 10 mM dNTP (Life Technologies/Thermo Fisher Scientific), and 0.1 µl SUPERase-In RNase-Inhibitor (20 U µl⁻¹, Life Technologies/Thermo Fisher Scientific). Samples were denatured at 72 °C for 3 min using an Eppendorf Mastercycler and placed immediately on ice afterwards. The Reverse Transcription Mix (7 µl) was subsequently added to every well, consisting of: 2 µl 5 × RT buffer (Thermo Fisher Scientific), 2 µl 5 M betaine (Sigma-Aldrich), 0.9 µl 100 mM MgCl₂ (Sigma-Aldrich), 1 µl 10 µM TSO (5'-AAGCAGTGGTATCAACGCAGAGTACATrGrG+G-3', Exiqon), 0.25 µl

SUPERase-In RNase-Inhibitor (20 U μl^{-1} , Life Technologies/Thermo Fisher Scientific), 0.1 μl Maxima H Minus Reverse Transcriptase (200 U μl^{-1} , Thermo Fisher Scientific) and 0.75 μl nuclease-free water. Reverse transcription was carried out by incubating the plate at 50 °C for 90 min, followed by heat inactivation at 85 °C for 5 min.

PCR pre-amplification and cDNA purification. PCR Mix (14 μl , consisting of 0.5 μl 10 μM PCR primer 5'-AAGCAGTGGTATCAACGCAGAGT-3' (IDT), 12.5 μl 2 \times KAPA HiFi HotStart ReadyMix (KAPA Biosystems) and 1 μl nuclease-free water) was added to each well for a final PCR reaction volume of 25 μl . The reaction was carried out with an initial incubation at 98 °C for 3 min, followed by 16 cycles at 98 °C for 15 s, 67 °C for 20 s, and 72 °C for 6 min, and a final extension at 72 °C for 5 min. PCR products were purified by mixing them with 20 μl (0.8 \times) of Agencourt AMPureXP SPRI beads (Beckman-Coulter), followed by a 6-min incubation period at room temperature. The plate was then placed onto a magnet for 6 min before removing the supernatant. SPRI beads were washed twice with 100 μl of freshly prepared 70% ethanol, with care being taken to avoid loss of beads during the washes. After removing all residual ethanol traces, SPRI beads were left to dry at room temperature for 10 min. The beads were then resuspended in 20 μl of TE buffer (Teknova) and incubated at room temperature for 5 min. The plate was placed on the magnet for 5 min before transferring the supernatant containing the amplified cDNA to a new 96-well plate. This cDNA SPRI clean-up procedure was repeated a second time to remove all residual primer dimers. The concentration of amplified cDNA was measured on the Synergy H1 Hybrid Microplate Reader (BioTek) using the Qubit dsDNA High Sensitivity Assay Kit (Life Technologies/Thermo Fisher Scientific). The cDNA size distribution of few selected wells was assessed on a High-Sensitivity Bioanalyzer Chip (Agilent), and the expected size distribution sharply peaked around 2 kb.

Sequencing library preparation. Library preparation was carried out using the Nextera XT DNA Sample Kit (Illumina) with custom indexing adapters, allowing the 18 libraries to be simultaneously generated in a 384-well PCR plate (Eppendorf). For each library, the amplified cDNA was normalized to a 0.15–0.20 ng μl^{-1} concentration range. The tagmentation reaction consisted of mixing 0.625 μl of normalized cDNA with 1.25 μl of Tagmentation DNA (TD) buffer and 0.625 μl of Amplicon Tagment enzyme Mix (ATM). The 2.5- μl reaction was incubated at 55 °C for 10 min and then immediately placed on ice upon completing this incubation step. The reaction was quenched with 0.625 μl of Neutralize Tagment (NT) buffer and incubated at room temperature for 10 min. The libraries were amplified by adding 1.875 μl of Nextera PCR Master (NPM) Mix, 0.625 μl of 10 μM i5 adaptor 5'-AATGATACGGCGACCACCGAGATCTACAC[i5]TCGTCGGCAGCGTC-3' (IDT), in which [i5] signifies the 8-bp i5 barcode sequence (see below for sequences), and 0.625 μl of 10 μM i7 adaptor 5'-CAAGCAGAAGACGGCATACGAGAT[i7]GTGACTGGAGTTCAGACGTGTGCTCTTCCGATCTGGG-3' (IDT), in which [i7] represents the reverse-complement of the 8-bp i7 barcode sequence (see below for sequences used). The PCR was carried out at an initial incubation at 72 °C for 3 min, 95 °C for 30 s, followed by 12 cycles of (95 °C for 10 s, 55 °C for 30 s, 72 °C for 1 min), and a final extension at 72 °C for 5 min. Following PCR amplification, 2.5 μl of each library were pooled together in a 1.5-ml Eppendorf tube. The pool was mixed with 67.5 μl (0.9 \times ratio for 2.5 μl of 30 samples pooled together) of Agencourt AMPureXP SPRI beads (Beckman-Coulter) and incubated at room temperature for 5 min. The pool was then placed on a magnet (DynaMag-2, Life Technologies) and incubated for 5 min. The supernatant was removed and the SPRI beads were washed twice with 1 ml of freshly prepared 70% ethanol. After removing all residual ethanol traces, the SPRI beads were left to dry at room temperature for 10 min. The beads were resuspended in 100 μl of nuclease-free water and incubated at room temperature for 5 min. The tube was then placed back on the magnet for 3 min before transferring the supernatant to a new 1.5-ml Eppendorf tube. This SPRI clean-up procedure of the library was repeated a second time to remove all residual primer dimers, using the same approach. The concentration of the pooled libraries was measured using the Qubit dsDNA High Sensitivity Assay Kit (Life Technologies/Thermo Fisher Scientific), and the library size distribution measured on a High-Sensitivity Bioanalyzer Chip (Agilent), showing the expected size distribution of 300–500 bp. The 18 pooled samples were sequenced as paired-end on an Illumina NextSeq 500 instrument using the NextSeq 500/550 High Output v2 kit (75 cycles).

i5 barcodes: AAGTAGAG, ACACGATC, TGTTCGGA. i7 barcodes: GAATTGCT, GTCAAGTT, ATCCGACA, CAAGGCGA, AGTGTCTT, GACCGAGA.

RNA sequencing analysis. Raw sequencing reads were demultiplexed and converted to FASTQ files using Illumina bcl2fastq2 Illumina software (version 2.17.1.14). FASTQ sequencing reads were then aligned to mm10 reference genome using the STAR aligner with default parameters⁴². RSEM (v.1.2.8) was used to quantify gene expression level from aligned reads and generate count expression matrices for each experimental condition⁴³. We filtered out lowly expressed genes with a count per million (CPM) < 0.5 in more than two conditions, leaving a total

of 14,168 genes for further analysis. The distribution of log₂ normalized CPM data was visualized to assess for coverage, and all conditions had similar distributions.

Gene expression analysis. Gene expression matrices were analysed using the limma package in R⁴⁴. The global topology of quantile normalized data was visualized using the multidimensional scaling (plotMDS) function in limma after removing batch effects using the removeBatchEffect function in limma with default parameters taking into account design and batch matrices. Differential gene expression was performed using empirical Bayesian statistics (eBayes) function in limma simultaneously correcting for batch using blocking terms for batch covariates. Differentially expressed genes with log fold change greater than 1 and a *P* value below cut-off were visualized using the heatmap.2 function in gplots. All *P* values were corrected for multiple hypothesis testing using Benjamini–Hochberg correction. For R scripts used to perform the gene expression analyses see Supplementary Methods. The same differential expression steps were used to re-analyse the gene expression data from GEO accession GSE82008 to obtain the list of differentially expressed genes between c-Rel and p65 knockout versus wild-type resting and activated T_{reg} cells. A list of 831 'eTreg signature' genes from ref.¹⁶ was obtained by direct correspondence with the authors. Overlap between differentially expressed genes, including the list of eT_{reg} cell signatures from the current study and ref.¹⁶, was visualized using the vennDiagram function in limma.

Quantitative RT–PCR. For analysis of gene expression, RNA was isolated (AllPrep, DNA/RNA Mini kit; Qiagen) from CD4⁺ GFP⁺ T_{reg} cells sorted to >99% purity from tdLNs and tumours, or from homogenized tumour tissue, and reverse transcribed using iScript cDNA Synthesis Kit (Bio-RAD). Quantitative reverse transcription (RT–PCR) was performed using iQ SYBR green supermix (Bio-RAD) and primers: CARMA1 Fwd 5'-ACATGCTGAGCCGTTACATCA-3', CARMA1 Rev 5'-CCACATAGCCCTTTGTCCC-3', *Ifng* Fwd 5'-CGGCACAGT CATTGAAAGCCTA-3', *Ifng* Rev 5'-GTTG CTGATGGCC TGATTGTC-3', *Ctla4* Fwd 5'-GCTTCCTAGATTACCCCTTCTGC-3', *Ctla4* Rev 5'-CGGGCATGG TTCTGGATCA-3', *CD25*-Fwd 5'-CCACATTCAAAGCC CTCTCCTA-3', *CD25*-Rev 5'-GTTTCCCACACTTCATCTTGC-3', *Foxp3* Fwd 5'-TTGG CCAGCGCCA TCTT-3', *Foxp3* Rev 5'-TGCCTCTCCAGAGAGAAGTG-3', *GITR* (also known as *Tnfrsf18*) Fwd 5'-AAGGTTCAAGACGGAAGTG-3', *GITR* Rev 5'-GGGTCTCCACAGTGGTACT-3', *CD73* (also known as *Nt5e*) Fwd 5'-CAA ATCCACACAACCACTG-3', *CD73* Rev 5'-TGCTCACTTGGTCACA GGAC-3', *Gzmb* Fwd 5'-CATGTAGGGTCGAGAGTGGG-3', *Gzmb* Rev 5'-CCTCCTGC TACTGCTGAC CT-3', *Pd1* (also known as *Cd274*) Fwd 5'-TGCTGCATAATCAGCTACGG-3', *Pd1* Rev 5'-GCTGGTCACATT GAGAAGCA-3', *Socs1*-Fwd 5'-ACAAGCTGCTACAACCAGG G-3', *Socs1* Rev 5'-ACT TCTGGCTGGAGACCTCA-3', *Tap1* Fwd 5'-GTGGCCGCAAGTG GGA CAAGAG-3', *Tap1* Rev 5'-AGGGCACTGGTGGCATCATC-3', *Stat1* Fwd 5'-TGGTGAAATTGCAAG AGCTG-3', *Stat1* Rev 5'-CAGACTTCCG TTGGTGGATT-3', *Irf1* Fwd 5'-CAG AGGAAAG AGAGAAAGTCC-3', *Irf1* Rev 5'-CACACGGTGACAGTGCTGG, *Cxcl10* Fwd 5'-CATC CTGCTGGGT CTGAGTG-3', *Cxcl10*-Rev 5'-ATTCTCACTGGCCCGTCATC, *Nos2* Fwd 5'-CAAGAGAGTGTCTTCCAGGT-3' and *Nos2* Rev 5'-GAGCAGCTGAGT ACC TCATT-3', *Gapdh* Fwd 5'-TGGTGAAGGTCGGTGAAC-3' and *Gapdh* Rev 5'-CC ATGTAGTTGAGGTCAATGAAGG-3'. Results were expressed as 2^{−ΔΔC_T} relative to the house keeping gene *Gapdh*.

Histology. Tissue samples obtained from all organs were fixed in 10% buffered formalin for 48 h, trimmed and placed into microcassettes, and embedded in paraffin wax. Sections of 5 μm were stained with haematoxylin and eosin according to standard procedures.

Immunofluorescence. Kidney, liver, and stomach from a *Rag1*^{−/−} mouse were embedded in OCT and flash-frozen in cold methylbutane equilibrated on dry ice. Sections of 10 μm were permeabilized with pre-cooled 90% methanol for 10 min at −20 °C, blocked in TruStain FcX (93, Biolegend) with 1% goat serum and 0.25% BSA in PBS for 60 min, incubated with sera (1:100 dilution) from *Foxp3*^{YFP-cre} \times *CARMA1*^{fl/fl} (or *CARMA1*^{fl/+} or *CARMA1*^{+/+}) mice for 120 min and stained with anti-mouse IgG (H+L)-Alexa Fluor 647 (1:500) (A-21235, Thermo Fisher) and DAPI (Sigma) for 120 min. Sections were mounted on coverslips in Prolong (Thermo Fisher) and imaged with LSM 780 AxioObserver confocal microscope (Carl Zeiss) using a 20 \times lens (Apochromat, 0.8 W).

Statistical analysis. A two-tailed Student's *t*-test was used for comparisons between two groups, and a two-way ANOVA with Bonferroni post hoc test (multiple time points) or one-way ANOVA with Tukey post hoc test (single time points) was used for comparisons across multiple groups, unless otherwise indicated. A log-rank (Mantel–Cox) test was used to compare survival curves. All statistical tests were performed with GraphPad Prism software, and *P* < 0.05 was considered statistically significant. No statistical methods were used to predetermine sample size. Investigators were not blinded to allocation during experiments and outcome assessment.

Reporting summary. Further information on research design is available in the Nature Research Reporting Summary linked to this paper.

Data availability

All datasets generated during the current study are available from the corresponding authors upon reasonable request. RNA sequencing data have been deposited at the Gene Expression Omnibus (GEO) under accession number GSE129480.

32. Rubtsov, Y. P. et al. Regulatory T cell-derived interleukin-10 limits inflammation at environmental interfaces. *Immunity* **28**, 546–558 (2008).
33. Rubtsov, Y. P. et al. Stability of the regulatory T cell lineage in vivo. *Science* **329**, 1667–1671 (2010).
34. Srinivas, S. et al. Cre reporter strains produced by targeted insertion of *EYFP* and *ECFP* into the *ROSA26* locus. *BMC Dev. Biol.* **1**, 4 (2001).
35. Sasaki, Y. et al. Canonical NF- κ B activity, dispensable for B cell development, replaces BAFF-receptor signals and promotes B cell proliferation upon activation. *Immunity* **24**, 729–739 (2006).
36. Dalton, D. K. et al. Multiple defects of immune cell function in mice with disrupted interferon- γ genes. *Science* **259**, 1739–1742 (1993).
37. Godfrey, V. L., Wilkinson, J. E., Rinchik, E. M. & Russell, L. B. Fatal lymphoreticular disease in the scurfy (sf) mouse requires T cells that mature in a sf thymic environment: potential model for thymic education. *Proc. Natl Acad. Sci. USA* **88**, 5528–5532 (1991).
38. Egawa, T. et al. Requirement for CARMA1 in antigen receptor-induced NF- κ B activation and lymphocyte proliferation. *Curr. Biol.* **13**, 1252–1258 (2003).
39. Marangoni, F. et al. The transcription factor NFAT exhibits signal memory during serial T cell interactions with antigen-presenting cells. *Immunity* **38**, 237–249 (2013).
40. Spiess, P. J., Yang, J. C. & Rosenberg, S. A. In vivo antitumor activity of tumor-infiltrating lymphocytes expanded in recombinant interleukin-2. *J. Natl. Cancer Inst.* **79**, 1067–1075 (1987).
41. Marangoni, F. et al. Tumor tolerance-promoting function of regulatory T cells is optimized by CD28, but strictly dependent on calcineurin. *J. Immunol.* **200**, 3647–3661 (2018).
42. Dobin, A. et al. STAR: ultrafast universal RNA-seq aligner. *Bioinformatics* **29**, 15–21 (2013).
43. Li, B. & Dewey, C. N. RSEM: accurate transcript quantification from RNA-Seq data with or without a reference genome. *BMC Bioinformatics* **12**, 323 (2011).
44. Ritchie, M. E. et al. limma powers differential expression analyses for RNA-sequencing and microarray studies. *Nucleic Acids Res.* **43**, e47 (2015).